Journal of Sound and Vibration 375 (2016) 386–402

Contents lists available at ScienceDirect

Journal of Sound and Vibration

journal homepage: www.elsevier.com/locate/jsvi

Simplified dispersion relationships for fluid-dominated axisymmetric wave motion in buried fluid-filled pipes

Yan Gao [a,*], Fusheng Sui [a], Jennifer M. Muggleton [b], Jun Yang [a]

[a] Key Laboratory of Noise and Vibration Research & State Key Laboratory of Acoustics, Institute of Acoustics, Chinese Academy of Sciences, Beijing 100190 China

[b] Institute of Sound and Vibration Research, University of Southampton, Highfield, Southampton SO17 1BJ, UK

ARTICLE INFO

Article history:
Received 7 December 2015
Received in revised form
10 April 2016
Accepted 12 April 2016
Handling Editor: L.G. Tham
Available online 25 April 2016

Keywords:
Axisymmetric waves
Dispersion
Buried fluid-filled pipes

ABSTRACT

The dispersion characteristics of axisymmetric ($n=0$) waves offer a way to gain physical insight into the low-frequency vibrational behaviour of underground pipe systems. Whilst these can be found in the literature, they are generally calculated numerically. Coupled equations of motion for the $n=0$ waves that propagate in a buried fluid-filled pipe are presented in this paper and, from this, an analytical solution is developed for the fluid-dominated ($s=1$) wavenumber. The effect of the frictional stress at the pipe–soil interface on the dispersion behaviour of the $s=1$ wave is characterised by adopting a soil loading matrix. Overall, the fluid loading has a greater effect on the propagation wavespeed compared with the soil loading: for metal pipes, the effect of soil loading is negligible; for plastic pipes, however, simply neglecting the effect of soil loading can lead to a considerable underestimation in the calculation of the wavespeed. The wave attenuation increases significantly at higher frequencies regardless of pipe material resulting from the added damping due to radiation into the soil. Theoretical predictions of the $s=1$ wavenumber are compared with experimental data measured on an MDPE water pipe. The degree of agreement between prediction and experiment makes clear that, although the wavespeed is only slightly affected by the presence of the frictional stress, the frictional stress at the pipe–soil interface needs to be appropriately taken into account for attenuation predictions.

© 2016 Elsevier Ltd. All rights reserved.

1. Introduction

Pipes are used all over the world for transporting fluids in many settings, for example in the petrochemical, water and energy industries. Leakage from such pipes is of major concern due to the potential social, environmental and economic consequences. As such, it is important not only to be able to detect leaks once they have occurred, but also to identify cracks and defects early on so that failures can be avoided. An important prerequisite to any of this is, of course, being able to identify the exact location of the pipe of interest – a simple process when the pipe is above ground but not always straightforward when the pipe in question is buried (and may have been buried for a number of decades).

Acoustic techniques can be extremely valuable in all of these areas. They are frequently used for detecting leaks, particularly in the water industry, where such methods have been effective and in common use over the past 30 years [1,2].

* Corresponding author.
E-mail address: gaoyan@mail.ioa.ac.cn (Y. Gao).

http://dx.doi.org/10.1016/j.jsv.2016.04.012
0022-460X/© 2016 Elsevier Ltd. All rights reserved.

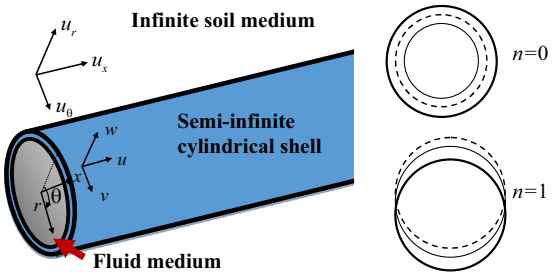

Fig. 1. The coordinate system for a buried fluid-filled pipe and mode shapes.

More recently they have been adopted to locate underground pipes [3,4] and characterize defects such as cracks, blockages and corrosion that may cause pipeline failure [5–8]. Understanding the acoustic characteristics of the dominant wave types which occur in pipes is vital to the success of any of these methods.

The frequency regimes of a fluid-filled pipe are separated by the pipe ring frequency (usually being a few kHz), which occurs when the circumference of the pipe equals a compressional wavelength. Below the pipe ring frequency, there are four wave types responsible for most of the energy transfer in fluid-filled pipes [9]: three $n=0$ waves and a bending ($n=1$) wave. The $n=0$ and $n=1$ mode shapes, along with the cylindrical coordinate system used for the analyses are shown in Fig. 1. Here, n and s denote the circumferential modal order and a particular branch order, representing a unique mode of propagation, respectively. Of the $n=0$ waves, two wave types are primarily longitudinal with some radial motion, denoted $s=1$, 2, which correspond to a fluid-dominated wave and an axial shell-dominated wave; and the third wave, $s=0$, is a torsional wave, which is uncoupled from the fluid and does not have significant radial motion. Axisymmetric ($n=0$) waves that propagate at low frequencies are particularly important for acoustic leak detection, the fluid-dominated ($s=1$) wave being largely responsible for the propagation of leak noise [10–12].

Much previous research has been devoted to studying the wave propagation and energy distribution within elastic fluid-filled pipes *in vacuo* [9,13–16]. A complete set of dispersion curves was presented by Fuller and Fahy [15] based on Donnell-Mushtari shell theory [17]. However, they do not provide expressions for $n=0$ wavenumbers *per se*. Based on the knowledge of the properties of axisymmetric, $n=0$, $s=1$, 2 waves, Pinnington and Briscoe [9] derived the approximate analytical solutions to the wavenumbers from the coupled pipe equations. In their model the shell bending is neglected, and thus the solutions are only valid below the pipe ring frequency. The possible $n=0$ waves that propagate in buried iron water pipes were also studied numerically by Long et al. [18] within the frequency range up to 25 kHz based on the DISPERSE model. The full solution to the $s=1$ wavespeed was compared with its analytical solution obtained by Muggleton et al. [19] (consistent with the results given in [9]) for a water-filled cast iron pipe *in vacuo*. As expected, the analytical solution agreed well with the full solution at frequencies below 2.5 kHz and deviates as it approaches the pipe ring frequency (calculated as 5640 Hz as illustrated in Fig. 3 in [18]).

Muggleton et al., in later work, [20] studied the axisymmetric wave propagation in a fluid-filled pipe surrounded by soil, with the application for the buried plastic water pipes. In this analysis, the effects of shear in the soil were considered and the $s=1$, 2 wavenumbers were derived under one extreme coupling condition, in which the frictional stress is presumed to be zero at the pipe–soil interface. Physically, this implies that the pipe–soil interface behaves as a pipe–fluid interface, although the surrounding soil supports the elastic waves. Of course, in reality, some frictional stresses will always be present at the interface. Slip or relative motion of pipe and soil at the interface commences only when the shear stress between the pipe and the surrounding soil reaches the value for limiting friction, this in turn being dependent on the static normal load on the pipe. The stresses (and strains) required to exceed limiting friction are large [21] and normally only occur in earthquake-type scenarios. Several numerical and analytical methods have been developed to investigate the vibrational behaviour of cylindrical underground structures [22] and the sliding at the interface when subjected to earthquake loading in seismic applications [23,24]. For the low-frequency, $n=0$ wave motion induced by water leaks, however, the dynamic strains will be small, so slippage is unlikely to occur. Therefore, it is more appropriate to assume that the pipe is in perfect bond with the soil such that there is no slippage between the soil and the pipe wall.

The present paper develops an analytical model to predict the low-frequency dispersion characteristics of the $n=0$, $s=1$ wave in a buried fluid-filled pipe. This work expands on previous investigations on a cylindrical shell filled with fluid [15], using the Donnell-Mushtari shell theory as a basis along with some additional assumptions adopted in [9] for the analysis of the propagating $s=1$ wave. It is set out as follows. Section 2 derives the coupled equations of motion for the $n=0$ waves for a thin-walled shell surrounded by an elastic medium. A simplified characteristic equation is further obtained and from this an expression for the $s=1$ wavenumber is formulated in Section 3. Section 4 presents some numerical results of the propagation wavespeed and attenuation for buried water pipes. In Section 5 the theoretical predictions are compared with experimental measurements. Finally, some conclusions are drawn in Section 6.

2. Equations of motion

This section derives the coupled equations of motion for the $n=0$ waves. Fuller and Fahy [15] have investigated the effect of an internal fluid by defining a fluid loading term, *FL*, in the equations of motion for a fluid-filled pipe *in vacuo*; we use this as a starting point for the current investigations. Here, however, we also introduce a soil loading matrix **SL** to characterize the coupling effect due to the presence of the surrounding soil.

Referring to the cylindrical co-ordinates as illustrated in Fig. 1, u, v and w denote the shell displacements in the x, θ and r directions, respectively; u_x, u_θ and u_r denote the soil displacements. The pipe has a mean radius a and wall thickness h, and is assumed to be thin such that $h/a \ll 1$. The internal fluid is assumed to be inviscid and the surrounding soil is assumed to be elastic, homogenous and isotropic. Both the fluid and the surrounding soil are assumed to be lossless.

2.1. Free vibrations of the fluid-filled pipe

Free vibrations of the fluid-filled pipe are described by the Donnell-Mushtari shell equations. Important assumptions used in deriving the Donnell-Mushtari equations are that the wall thickness is thin with respect to the smallest wavelength considered; moreover, the variations in transverse shear and the rotary inertia of the element are ignored. Equations of motion of free vibrations of the coupled system can be represented in matrix form as [17]

$$\begin{bmatrix} A_{11} & A_{12} & A_{13} \\ A_{21} & A_{22} & A_{23} \\ A_{31} & A_{32} & A_{33} \end{bmatrix} \begin{pmatrix} u \\ v \\ w \end{pmatrix} = \frac{1-\nu_p^2}{Eh} \begin{pmatrix} 0 \\ 0 \\ p_f(a) \end{pmatrix} \tag{1}$$

where $A_{11} = \frac{\partial^2}{\partial x^2} + \frac{1-\nu_p}{2a^2}\frac{\partial^2}{\partial \theta^2} - \frac{\rho_p(1-\nu_p^2)}{E_p}\frac{\partial^2}{\partial t^2}$; $A_{12} = \frac{1+\nu_p}{2a}\frac{\partial^2}{\partial x \partial \theta}$; $A_{13} = \frac{\nu_p}{a}\frac{\partial}{\partial x}$; $A_{21} = A_{12}$; $A_{22} = \frac{1-\nu_p}{2}\frac{\partial^2}{\partial x^2} + \frac{1}{a^2}\frac{\partial^2}{\partial \theta^2} - \frac{\rho_p(1-\nu_p^2)}{E_p}\frac{\partial^2}{\partial t^2}$; $A_{23} = \frac{1}{a^2}\frac{\partial}{\partial \theta}$; $A_{31} = A_{13}$; $A_{32} = A_{23}$; $A_{33} = \frac{1}{a^2} + \delta^2 a^2 \nabla^4 + \frac{\rho_p(1-\nu_p^2)}{E_p}\frac{\partial^2}{\partial t^2}$; $\nabla^4 = \frac{\partial^4}{\partial x^4} + \frac{2}{a^2}\frac{\partial^4}{\partial x^2 \partial \theta^2} + \frac{1}{a^4}\frac{\partial^4}{\partial \theta^4}$. Here, ρ_p, E_p and ν_p are the density, Young's modulus and Poisson's ratio of the shell; δ is the stiffness factor, $\delta^2 = h^2/12a^2$; $p_f(a)$ is the internal pressure at the pipe–fluid interface $r=a$. The shell equations consist of three coupled equations for each axis of motion which must be solved simultaneously. For $n=0$ motion, the variations with respect to θ vanish ($\partial/\partial\theta = 0$) in the matrix **A**, and thereby it can be seen that the axial and radial motion is uncoupled from rotational motion. The coupled equations of motion in the axial and radial directions become

$$\begin{bmatrix} A_{11} & A_{13} \\ A_{31} & A_{33} \end{bmatrix} \begin{pmatrix} u \\ w \end{pmatrix} = \frac{1-\nu_p^2}{E_p h} \begin{pmatrix} 0 \\ p_f(a) \end{pmatrix} \tag{2}$$

where

$$A_{11} = \frac{\partial^2}{\partial x^2} - \frac{\rho_p(1-\nu_p^2)}{E_p}\frac{\partial^2}{\partial t^2};\ A_{13} = \frac{\nu_p}{a}\frac{\partial}{\partial x};\ A_{31} = A_{13};\ A_{33} = \frac{1}{a^2} + \delta^2 a^2 \frac{\partial^4}{\partial x^4} + \frac{\rho_p(1-\nu_p^2)}{E_p}\frac{\partial^2}{\partial t^2}.$$

2.2. Soil vibration

Consider the fluid-filled pipe to be surrounded by an elastic medium which can sustain two types of elastic waves, compressional and shear. For the $n=0$ motion considered (i.e., the coupled axial and radial motion), the circumferential displacement vanishes ($u_\theta = 0$), as do the circumferential shear stress ($\tilde{\sigma}_{r\theta} = 0$) and variations with respect to θ ($\partial/\partial\theta = 0$). The soil displacements, u_x and u_r, satisfy the following two equations of motion [25]

$$\rho_m \frac{\partial^2 u_x}{\partial t^2} = (\lambda_m + 2\mu_m)\left(\frac{\partial^2 u_r}{\partial x \partial r} + \frac{\partial u_r}{r \partial x} + \frac{\partial^2 u_x}{\partial x^2}\right) - \frac{\mu_m}{r}\left(\frac{\partial u_r}{\partial x} - \frac{\partial u_x}{\partial r}\right) - \mu_m\left(\frac{\partial^2 u_r}{\partial x \partial r} - \frac{\partial^2 u_x}{\partial r^2}\right)$$

$$\rho_m \frac{\partial^2 u_r}{\partial t^2} = (\lambda_m + 2\mu_m)\left(\frac{\partial^2 u_r}{\partial r^2} + \frac{\partial u_r}{r \partial r} - \frac{u_r}{r^2} + \frac{\partial^2 u_x}{\partial x \partial r}\right) + \mu_m\left(\frac{\partial^2 u_r}{\partial x^2} - \frac{\partial^2 u_x}{\partial x \partial r}\right) \tag{3a, b}$$

where ρ_m, λ_m and μ_m are the density and Lamé coefficients of the surrounding soil. The corresponding soil displacements in cylindrical coordinates may be expressed in terms of two potentials by [25]

$$u_x = \frac{\partial \phi_m}{\partial x} - \frac{\partial^2 \psi_m}{\partial r^2} - \frac{\partial \psi_m}{r \partial r};\ u_r = \frac{\partial \phi_m}{\partial r} + \frac{\partial^2 \psi_m}{\partial x \partial r} \tag{4a, b}$$

where ϕ_m and ψ_m are the compressional and shear wave potentials respectively. Substituting Eqs. (4a, b) into (3a, b), it can be found that the compressional and shear wave potentials must satisfy [25]

$$\nabla^2 \phi_m = \frac{1}{c_d^2}\frac{\partial^2 \phi_m}{\partial t^2};\ \nabla^2 \psi_m = \frac{1}{c_r^2}\frac{\partial^2 \psi_m}{\partial t^2} \tag{5a, b}$$

where c_d and c_r are the propagation wavespeeds, $c_d = \sqrt{(\lambda_m + 2\mu_m)/\rho_m}$ and $c_r = \sqrt{\mu_m/\rho_m}$, the subscripts d and r referring to

the dilatational (i.e., compressional) and rotational (i.e., shear) waves respectively. For each s wave, the travelling wave solutions to Eqs. (5a, b) can be expressed using Hankel function of the second kind and zero order, $H_0(\ )$, as

$$\phi_m = A_m H_0(k_{ds}^r r) e^{i(\omega t - k_s x)};\ \psi_m = B_m H_0(k_{rs}^r r) e^{i(\omega t - k_s x)} \tag{6a, b}$$

where A_m and B_m are potential coefficients; $H_0(k_{ds}^r r)$ and $H_0(k_{rs}^r r)$, represent conical waves radiating outward from the pipe into the surrounding soil; the radial wavenumbers, k_{ds}^r and k_{rs}^r, are related to the compressional and shear wavenumbers in the surrounding medium, k_d and k_r, by $(k_{ds}^r)^2 = k_d^2 - k_s^2$ and $(k_{rs}^r)^2 = k_r^2 - k_s^2$ respectively; k_s is the axial wavenumber; and ω is the angular frequency. Substituting Eqs. (6a, b) into Eqs. (4a, b) gives

$$\begin{pmatrix} u_x \\ u_r \end{pmatrix} = \mathbf{T}_1 \begin{pmatrix} A_m \\ B_m \end{pmatrix} e^{i(\omega t - k_s x)} \tag{7}$$

where $\mathbf{T}_1 = \begin{bmatrix} -ik_s H_0(k_{ds}^r r) & (k_{rs}^r)^2 H_0(k_{rs}^r r) \\ k_{ds}^r H_0'(k_{ds}^r r) & -ik_s k_{rs}^r H_0'(k_{rs}^r r) \end{bmatrix}$; and $H_0' = (\partial/\partial r) H_0(\ )$. According to Hooke's Law, the stresses are related to the soil displacements by

$$\tilde{\sigma}_{rx} = \mu_m \left(\frac{\partial u_r}{\partial x} + \frac{\partial u_x}{\partial r} \right);\ \tilde{\sigma}_{rr} = \lambda_m \Delta + 2\mu_m \frac{\partial u_r}{\partial r} \tag{8a, b}$$

where Δ is the dilation, $\Delta = \nabla^2 \phi_m = \frac{1}{r}\frac{\partial}{\partial r}\left(r \frac{\partial \phi_m}{\partial r} \right) + \frac{\partial^2 \phi_m}{\partial x^2}$ [25]. Substituting Eqs. (6a) and (7) into Eqs. (8a, b) gives

$$\begin{pmatrix} \tilde{\sigma}_{rx} \\ \tilde{\sigma}_{rr} \end{pmatrix} = \mathbf{T}_2 \begin{pmatrix} A_m \\ B_m \end{pmatrix} e^{i(\omega t - k_s x)} \tag{9}$$

where $\mathbf{T}_2 = \begin{bmatrix} -2i\mu_m k_s k_{ds}^r H_0'(k_{ds}^r r) & -\mu_m k_{rs}^r (2k_s^2 - k_r^2) H_0'(k_{rs}^r r) \\ 2\mu_m (k_{ds}^r)^2 H_0''(k_{ds}^r r) - \lambda_m k_d^2 H_0(k_{ds}^r r) & -2i\mu_m k_s (k_{rs}^r)^2 H_0''(k_{rs}^r r) \end{bmatrix}$; and $H_0'' = (\partial^2/\partial^2 r) H_0(\ )$. Combining Eqs. (7) and (9) and eliminating the potential coefficients A_m and B_m, the stresses $\tilde{\sigma}_{rx}$ and $\tilde{\sigma}_{rr}$ can be expressed in terms of soil displacements u_x and u_r by

$$\begin{pmatrix} \tilde{\sigma}_{rx} \\ \tilde{\sigma}_{rr} \end{pmatrix} = \mathbf{T} \begin{pmatrix} u_x \\ u_r \end{pmatrix} \tag{10}$$

where $\mathbf{T}$ is a 2×2 matrix, $\mathbf{T} = \mathbf{T}_2 \mathbf{T}_1^{-1}$, and the elements of which are given by

$$T_{11} = \frac{\mu_m}{a} \frac{k_{ds}^r a k_{rs}^2 a^2}{k_{rs}^r a k_{ds}^r a [H_0(k_{rs}^r a)/H_0'(k_{rs}^r a)] + k_s^2 a^2 [H_0(k_{ds}^r a)/H_0'(k_{ds}^r a)]}$$

$$T_{12} = -i\mu_m k_s \left\{ 2 - \frac{k_r^2 a^2 H_0(k_{ds}^r a)/H_0'(k_{ds}^r a)}{k_{rs}^r a k_{ds}^r a [H_0(k_{rs}^r a)/H_0'(k_{rs}^r a)] + k_s^2 a^2 [H_0(k_{ds}^r a)/H_0'(k_{ds}^r a)]} \right\}$$

$$T_{21} = -T_{12}$$

$$T_{22} = -\frac{\mu_m}{a} \left\{ 2 + \frac{k_{rs}^r a k_{rs}^2 a^2 [H_0(k_{rs}^r a)/H_0'(k_{rs}^r a)][H_0(k_{ds}^r a)/H_0'(k_{ds}^r a)]}{k_{rs}^r a k_{ds}^r a [H_0(k_{rs}^r a)/H_0'(k_{rs}^r a)] + k_s^2 a^2 [H_0(k_{ds}^r a)/H_0'(k_{ds}^r a)]} \right\} \tag{11a–d}$$

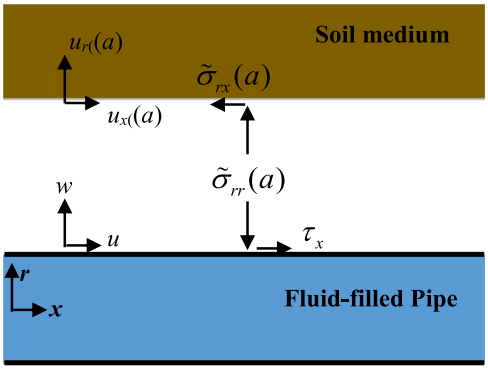

Fig. 2. Displacements and stresses acting at the pipe–soil interface.

2.3. Coupled equations of motion

Referring to Fig. 2, for the $n=0$ motion considered above, the soil applies the the stress $\tilde{\sigma}_{rr}(a)$ along the pipe surface in the radial direction; the frictional stress along the pipe surface τ_x equals the shear stress $\tilde{\sigma}_{rx}(a)$ along the pipe surface in the axial direction. As a result, the coupled equations of motion given by Eq. (2) become

$$\begin{bmatrix} A_{11} & A_{13} \\ A_{31} & A_{33} \end{bmatrix} \begin{pmatrix} u \\ w \end{pmatrix} = \frac{1-\nu_p^2}{E_p h} \begin{pmatrix} -\tau_x \\ p_f(a)+\tilde{\sigma}_{rr}(a) \end{pmatrix} \tag{12}$$

Travelling wave solutions of the equations of motion for each s wave, may be assumed to have the form

$$u = U_s e^{i(\omega t - k_s x)};\ w = W_s e^{i(\omega t - k_s x)} \tag{13a, b}$$

where U_s and W_s are the amplitudes of shell displacements in the axial and radial directions respectively. Substituting Eqs. (13a, b) into (12) gives

$$\begin{bmatrix} \Omega^2 - (k_s a)^2 & -i\nu_p(k_s a) \\ -i\nu_p(k_s a) & 1-\Omega^2+\beta^2(k_s a)^4 \end{bmatrix} \begin{pmatrix} u \\ w \end{pmatrix} = \frac{1-\nu_p^2}{E_p h} a^2 \begin{pmatrix} -\tau_x \\ p_f(a)+\tilde{\sigma}_{rr}(a) \end{pmatrix} \tag{14}$$

where Ω is the nondimensional frequency, $\Omega = k_L a$; k_L is the shell compressional wavenumber, $k_L^2 = \omega^2 \rho_p (1-\nu_p^2)/E_p$. For a thin-walled pipe $h/a = 0.05$, $\delta^2 = 2.1 \times 10^{-4}$. The product of $\delta^2 (k_s a)^4$ is very small since the frequency range of interest is well below the ring frequency and thus it can be ignored. It is clear from Eq. (14) that to obtain the dispersion relationship for the s wave, the boundary conditions at the interfaces must be defined; this then enables the internal pressure p_f(a) and the stresses τ_x and $\tilde{\sigma}_{rr}(a)$ applied along the pipe to be expressed in terms of the shell displacements u and w.

2.3.1. Pressure at the pipe–fluid interface

Applying the momentum equation and ensuring and displacement continuity in the radial direction at $r=a$, the pressure $p_f(a)$ is given by [15]

$$p_f(a) = \frac{\omega^2 \rho_f J_0(k_{fs}^r a)}{k_{fs}^r J_0'(k_{fs}^r a)} w \tag{15}$$

where, J_0 is a Bessel function of order zero, representing the internal fluid field, the internal fluid radial wavenumber, k_{fs}^r, is related to the fluid wavenumber, k_f, by $(k_{fs}^r)^2 = k_f^2 - k_s^2$ and $k_f = \omega/c_f$; c_f is the free-field fluid wavespeed, $c_f = \sqrt{B_f/\rho_f}$; B_f and ρ_f are the bulk modulus and density of the internal fluid; and $J_0' = (\partial/\partial r) J_0(\ )$. Eq. (15) shows that the internal pressure $p_f(a)$ is directly proportional to the radial displacement of the pipe wall, w, since a fluid does not support shear.

2.3.2. Stresses at the pipe–soil interface

The boundary conditions at the pipe/soil interface are less easy to determine. Here we consider two extremes: that of "compact contact", when the pipe wall is in perfect bond with the soil; and that of "lubricated contact" [20].

When the pipe is in perfect bond with the soil, there is no relative motion at the pipe–soil interface, and continuity of displacement must be satisfied in both the axial and radial directions, i.e., $u = u_x(a)$ and $w = u_r(a)$. Noting $\tau_x = \tilde{\sigma}_{rx}(a)$, the stresses τ_x and $\tilde{\sigma}_{rr}(a)$ are obtained from Eq. (10) by

$$\begin{pmatrix} \tau_x \\ \tilde{\sigma}_{rr}(a) \end{pmatrix} = \mathbf{T} \begin{pmatrix} u \\ w \end{pmatrix} \tag{16}$$

which relates the stresses τ_x and $\tilde{\sigma}_{rr}(a)$ along the pipe wall to the shell displacements u and w.

For lubricated contact [20], the displacement continuity condition is still satisfied in the radial direction, i.e. $w = u_r(a)$; however, there is no frictional stress applied in the axial direction $\tau_x = 0$, so the shear stress also vanishes along the soil interface, i.e., $\tilde{\sigma}_{rx}(a) = 0$. Physically, the soil motion in the axial direction is unconstrained under this assumption.

Table 1
Properties of the pipe, soil and water.

Properties	Cast iron	PVC	Soil A	Soil B	Water
Density (kg/m^3)	7100	2000	2000	2000	1000
Young's modulus (N/m^2)	1e11	5.0e9	–	–	–
Bulk's modulus (N/m^2)	–	–	5.3e7	4.5e9	2.25e9
Shear modulus (N/m^2)	–	–	2e7	1.8e8	–
Poisson's ratio	0.29	0.4	–	–	–
Material loss factor	0.001	0.065	–	–	–

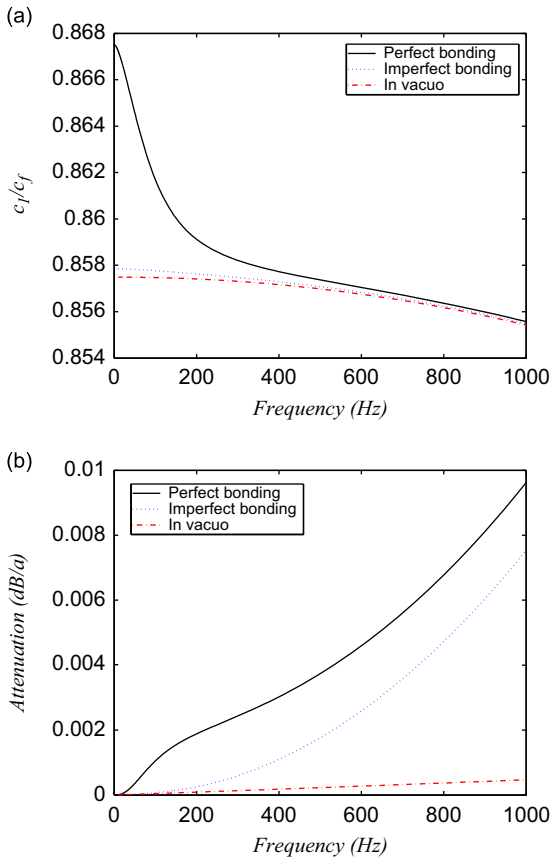

Fig. 3. Dispersion curves for the $s=1$ wave in a cast iron water pipe buried in sandy soil (A): (a) normalised wavespeed; (b) attenuation (dB/a).

From Eq. (10), the stress $\tilde{\sigma}_{rr}(a)$ can be found to be

$$\tilde{\sigma}_{rr}(a) = \left(-\frac{T_{12}T_{21}}{T_{11}} + T_{22}\right) w \tag{17}$$

Subsituting Eqs. (11a–d) into (17) gives

$$\tilde{\sigma}_{rr}(a) = -\frac{\mu_m}{a}\left[2 + \frac{(k_r^2 a^2 - 2k_s^2 a^2)^2}{k_r^2 a^2 k_{ds}^r a}\frac{H_0(k_{ds}^r a)}{H_0'(k_{ds}^r a)} + 4k_{rs}^r a \frac{k_s^2 a^2}{k_r^2 a^2}\frac{H_0(k_{rs}^r a)}{H_0'(k_{rs}^r a)}\right] w \tag{18}$$

Similar to the internal pressure $p_f(a)$ given by Eq. (15), it can be seen from Eq. (18) that the stress $\tilde{\sigma}_{rr}(a)$ applied by the soil only depends upon the radial displacement of the pipe wall w. Therefore, the pipe–soil interface under lubricated contact can be considered to behave as a pipe–fluid interface.

2.3.3. *Soil loading vs fluid loading*

Under the "perfect bonding" boundary condition, we substitute Eqs. (15) and (16) into Eq. (14). By neglecting the product $\delta^2(k_s a)^4$ and eliminating the harmonic terms $e^{i(\omega t - k_s x)}$, the coupled equations of motion for the axisymmetric s wave in a buried fluid-filled pipe are obtained in compact form as

$$\begin{bmatrix} L_{11} & L_{13} \\ L_{31} & L_{33} \end{bmatrix} \begin{pmatrix} U_s \\ W_s \end{pmatrix} = \mathbf{0} \tag{19}$$

where the elements of the matrix $\mathbf{L}$ are given by

$$\begin{aligned} L_{11} &= \Omega^2 - (k_s a)^2 - SL_{11} \\ L_{13} &= -i\nu_p(k_s a) - SL_{12} \\ L_{31} &= -i\nu_p(k_s a) - SL_{21} \\ L_{33} &= 1 - \Omega^2 - FL - SL_{22} \end{aligned} \tag{20a-d}$$

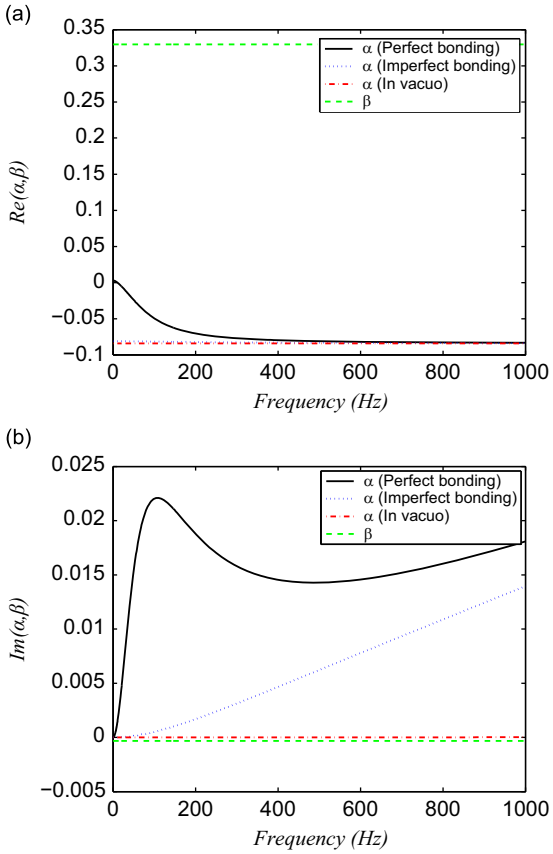

Fig. 4. Measures of the effects of soil and fluid loading, α and β, for a cast iron water pipe buried in sandy soil (A): (a) real part; (b) imaginary part.

The fluid loading term, *FL*, (first introduced by Fuller and Fahy [15]) and the soil loading matrix, **SL**, represent the coupling effects of the fluid and soil respectively, and are given by

$$FL = \frac{\rho_f}{\rho_p}\frac{a}{h}\frac{\Omega^2}{k_{fs}^r a}\frac{\mathrm{J}_0(k_{fs}^r a)}{\mathrm{J}_0'(k_{fs}^r a)} \tag{21}$$

and

$$\mathbf{SL} = \frac{(1-\nu_p^2)}{E_p}\frac{a^2}{h}\begin{bmatrix} -T_{11} & -T_{12} \\ T_{21} & T_{22} \end{bmatrix} \tag{22}$$

Applying the approximation for the Bessel function ratio at low frequencies, given in the Appendix, Eq. (21) becomes

$$FL = -2\frac{\rho_f}{\rho_p}\frac{a}{h}\frac{\Omega^2}{k_f^2 a^2 - k_s^2 a^2} \tag{23}$$

For "imperfect bonding" we substitute Eqs. (15), (18) into (14). This again leads to the coupled equations of motion Eq. (19) but here with the soil loading matrix obtained by

$$SL_{11} = 0; SL_{12} = 0; SL_{21} = 0;$$
$$SL_{22} = -\mu_m\frac{(1-\nu_p^2)}{E_p}\frac{a}{h}\left\{2 + \frac{(k_r^2 a^2 - 2k_s^2 a^2)^2}{k_r^2 a^2 k_{ds}^r a}\frac{H_0(k_{ds}^r a)}{\mathrm{H}_0'(k_{ds}^r a)} + 4k_{rs}^r a\frac{k_s^2 a^2}{k_r^2 a^2}\frac{H_0(k_{rs}^r a)}{\mathrm{H}_0'(k_{rs}^r a)}\right\} \tag{24a-d}$$

3. Approximate $s=1$ wavenumber

The non-trivial solutions to the *s* wavenumbers, for either soil coupling condition, can be obtained from the characteristic equation, i.e., by setting the determinant of the matrix **L** in the coupled equations of motion to zero. Analytical solutions are not straightforward to obtain. However, some approximations may be made which make the characteristic equation more tractable. For the $s=1$ wavenumber, it is assumed that k_1 is much larger than the shell compressional wavenumber k_L,

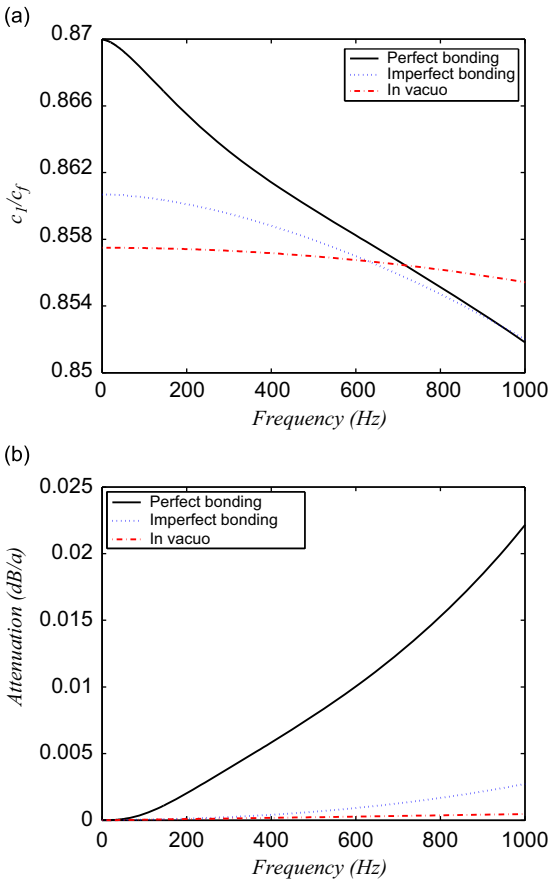

Fig. 5. Dispersion curves for the $s=1$ wave in a cast iron water pipe buried in clay soil (B): (a) normalised wavespeed; (b) attenuation (dB/a).

i.e., $k_1^2 >> k_L^2$ [9]. Setting $\det[\mathbf{L}(k_s^2)]=0$ and noting $(k_1 a)^2 \gg \Omega^2$, the simplified characteristic equation which describes the propagation of the $s=1$ wave becomes

$$1-\Omega^2-FL-SL_{22}-\frac{(v_p-\mathrm{i}SL_{12}/k_1 a)^2}{1+SL_{11}/k_1^2 a^2}=0 \tag{25}$$

Substituting the fluid loading term FL given by Eq. (23) into Eq. (25) and rearranging gives the approximate solution to the complex $s=1$ wavenumber as

$$k_1^2=k_f^2\left(1+\frac{\beta}{1-\Omega^2+\alpha}\right) \tag{26}$$

where α and β are measures of the effects of soil and fluid loading on the pipe wall, and given by

$$\alpha=-SL_{22}-\frac{(v_p-\mathrm{i}SL_{12}/k_1 a)^2}{1+SL_{11}/k_1^2 a^2};\ \beta=2\frac{B_f a}{E_p h}(1-v_p^2) \tag{27a, b}$$

respectively. From Eq. (27b), the fluid loading term, β, can be determined in a straightforward manner. It remains to determine the soil loading, α, given by Eq. (27a); this must be calculated recursively since it is a function of the wavenumber k_1. Thus no simple formulae can be further obtained to quantify the effect of the soil loading on the acoustic characteristics of the $s=1$ wave. Clearly the complex α leads to a complex value of k_1^2. Taking the square root of k_1^2 gives rise to a complex wavenumber k_1, the real and imaginary parts of which give the wavespeed and attenuation respectively. Consider the following soil coupling conditions:

(1) For the fluid-filled pipe *in vacuo*, setting $\mathbf{SL}=\mathbf{0}$ in Eq. (27a) gives $\alpha=-v_p^2$. As a result, the $s=1$ wavenumber given by Eq. (26) becomes

$$k_1^2=k_f^2\left(1+\frac{\beta}{1-v_p^2-\Omega^2}\right) \tag{28}$$

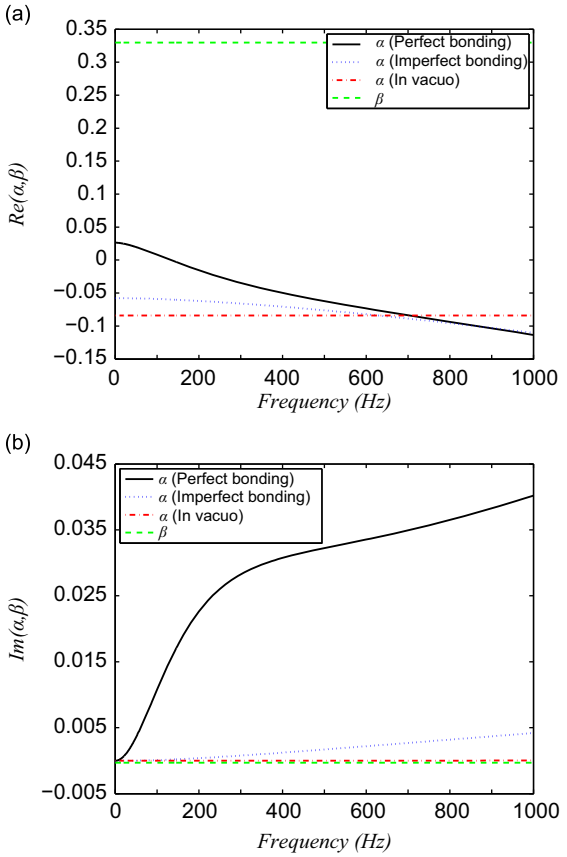

Fig. 6. Measures of the effects of soil and fluid loading, α and β, for a cast iron water pipe buried in clay soil (B): (a) real part; (b) imaginary part.

This is consistent with the result represented in [9, Eq. (13)]. It can be seen that at lower frequencies ($\Omega^2 \ll 1$) the $s=1$ wave always travels slower than the free-field fluid wavespeed c_f (i.e., $k_1^2 > k_f^2$) due to the effect of the fluid loading term, β. The $s=1$ wavespeed decreases with frequency (increasing Ω^2) and with decreasing the pipe wall stiffness (increasing β).

(2) For a buried fluid-filled pipe under lubricated contact, Eq. (27a) reduces to $\alpha = -v_p^2 - SL_{22}$. Substituting SL_{22} from Eqs. (24d) into (26), after some manipulation, leads to the same $s=1$ wavenumber presented in [20] (Eq. (36)). Similar to "perfect bonding", the resultant wavenumber k_1 for this case is always complex indicating the $s=1$ wave decays as it propagates in the fluid-filled pipe, whether or not there are losses within the pipe wall material. With reference to Eq. (26), the effect of the soil medium will be clarified further in the next section when compared with the *in vacuo* case.

4. Numerical results and discussions

This section presents some numerical examples. The effects of pipe material and soil loading are of particular interest. The results are also compared with the case of no surrounding soil. Losses within the pipe wall are included but the surrounding medium is assumed to be lossless. Both a metal (cast iron) and a plastic (PVC) pipe are considered, buried in each of two representative soils typical of sandy soil (A) and clay/chalky soil (B), to be consistent with Ref. [18]. The material properties of the pipe, soil and fluid are shown in Table 1. The $s=1$ wavenumbers are calculated up to 1 kHz. The wavespeeds are normalised by the free-field wavespeed c_f, and the attenuations are defined by the loss in dB per unit propagation distance (measured in pipe radii) by

$$\text{Loss(dB/unit distance } a) = -20\frac{\text{Im}\{k_s a\}}{\ln(10)} \tag{29}$$

4.1. Cast iron pipe

The normalised wavespeed and attenuation are shown in Fig. 3(a) and (b) for a cast iron pipe buried in sandy soil (A). It can be seen from Fig. 3(a) that without the surrounding soil (*in vacuo*), the $s=1$ wavespeed decreases slightly with frequency at the frequencies considered, compared with the free-field fluid wavespeed (1500 m/s). At low frequencies ($\Omega^2 \ll 1$),

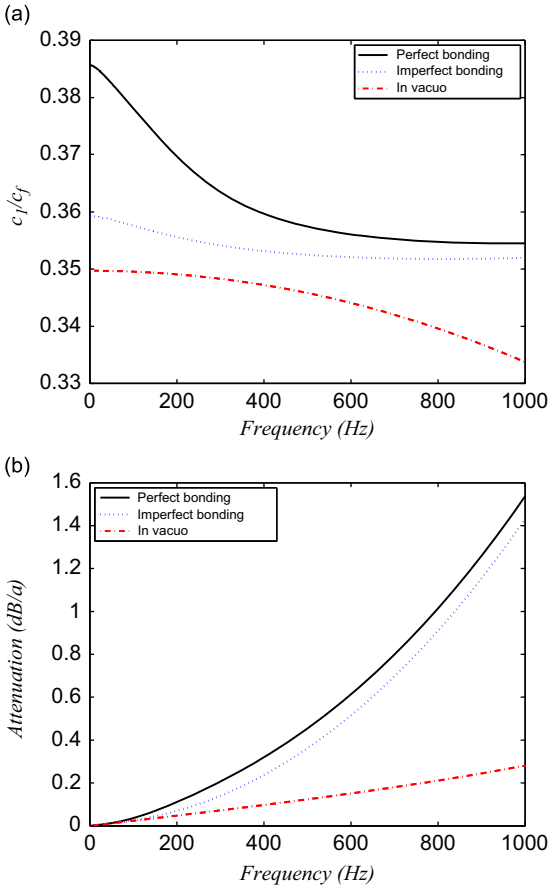

Fig. 7. Dispersion curves for the $s=1$ wave in a PVC water pipe buried in sandy soil (A): (a) normalised wavespeed; (b) attenuation (dB/a).

Eq. (26) reduces to

$$k_1^2 = k_f^2\left(1+\frac{\beta}{1-\nu_p^2}\right) \tag{30}$$

from which the $s=1$ wavespeed can be approximated by

$$c_1 = c_f\left(1+\frac{2B_f a}{E_p h}\right)^{-1/2} \tag{31}$$

This is the well known Korteweg equation given in [26]. For the cast iron pipe filled with water, the fluid loading, $\mathrm{Re}(\beta)=0.33$, is less than unity. The fluid loading term in Eq. (30), $\mathrm{Re}(\beta/1-\nu_p^2)<1$, indicating that the fluid loading is light. Eq. (31) provides a good approximation of the $s=1$ wavespeed for the cast iron water pipe *in vacuo*, $c_1=0.86c_f$, as shown in Fig. 3(a). Hence the $s=1$ wave can be considered to be non-dispersive at low frequencies. It can be seen from Fig. 3(a), for a buried fluid-filled pipe under both bonding conditions, the effect of the surrounding soil is to increase the wavespeed, particularly at lower frequencies, with the effect being larger for "perfect bonding", relative to the *in vacuo* case. Nonetheless, except at very low frequencies for "perfect bonding" (where there is a slight increase in the wavespeed except for an error up to $0.01c_f$ for "perfect bonding"), Eq. (31) still results in good approximation of the wavespeed. As can be seen in Fig. 4(a), for both bonding conditions, the real parts of α, $\mathrm{Re}(\alpha)$, decrease with frequency more markedly for "perfect bonding", and approach the *in vacuo* value, $\alpha=-\nu_p^2$ (calculated as -0.084) at high frequencies. $\mathrm{Re}(\alpha)$ is considerably smaller than $\mathrm{Re}(\beta)$, suggesting that the propagation wavespeed is mainly affected by the fluid loading; furthermore, in this case, the effect of soil loading can be neglected in the calculation of the propagation wavespeed.

Loss within the pipe wall is represented by a complex elastic modulus, $E_p(1+i\eta)$, where η is the material loss factor given in Table 1. As can be seen from Eq. (30), without the surrounding soil, the attenuation is governed by the material losses. Fig. 3(b) shows that the attenuation for the *in vacuo* pipe varies approximately linearly with frequency; this is as expected since the imaginary part of β, $\mathrm{Im}(\beta)$, (shown in Fig. 4(b))is frequency invariant. When the pipe is surrounded by a soil medium, it can be seen from Eq. (29) that the attenuation arises from both material losses within the pipe wall and radiation losses due to the added damping effect of soil loading. Fig. 4(b) shows the soil loading component, $\mathrm{Im}(\alpha)$, has major

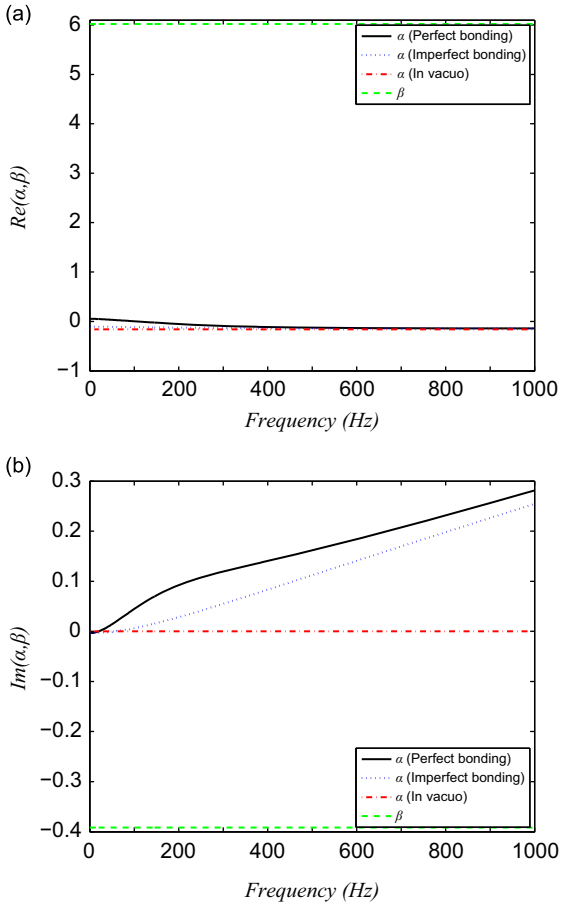

Fig. 8. Measures of the effects of soil and fluid loading, α and β, for a PVC water pipe buried in sandy soil (A): (a) real part; (b) imaginary part. Plot of α for Perfect bonding (----), Imperfect bonding (·····), and *In vacuo* (·-·-·); Plot of β (- - -).

influence on the attenuation, in particular, for "perfect bonding", in that Im(α) is much greater than Im(β) throughout the frequency range of interest. Correspondingly, as shown in Fig. 3(b), for the cast iron pipe buried in sand soil (A), the "perfect bonding" results in a marked increase of the attenuation compared to "imperfect bonding" as a result of the soil loading.

A similar trend can be found in the wavespeeds plotted in Fig. 5(a) for the cast iron pipe buried in clay soil (B). The effect of soil loading leads to an increase in the wavespeeds for both bonding conditions at lower frequencies; however, at higher frequencies a decrease is observed compared with the *in vacuo* case. The real parts of α and β are plotted in Fig. 6(a). As can be seen from the figure, "perfect bonding" results in a larger change in Re(α) compared to "imperfect bonding". For both bonding conditions, Re(α) drops below the value of the *in vacuo* case $\alpha = -\nu_p^2$ at higher frequencies. For the light fluid loading seen here, Re(α), regardless of the surrounding medium, is relatively small compared with Re(β). Thus it is anticipated that the propagation wavespeed is unlikely to be significantly affected by the presence of the surrounding soil. Figs. 3(a) and 5(a) show that, indeed, a good approximation of the wavespeed can always be obtained using Eq. (31) for a metal pipe; this is regardless of the soil properties and pipe–soil coupling conditions.

Turning our attention to the wave attenuation, comparing Figs. 3(b) and 5(b), it is found that the attenuation is greatly altered by the soil loading, with the largest being in clay soil (B) for "perfect bonding" and the smallest in sandy soil (A) for "imperfect bonding". The effect of the soil loading on the attenuation can be readily explained with reference to Figs. 4 (b) and 6(b). For both coupling conditions, the attenuation can be seen to be dominated by the added damping due to the soil loading, as Im(α) is much greater than Im(β). In turn, Im(α) is controlled both by the soil properties and the pipe–soil coupling conditions.

4.2. PVC pipe

The dispersion curves for the $s=1$ wave are plotted for the PVC water pipe in Fig. 7 for sandy soil (A) and in Fig. 9 for clay soil (B). Figs. 8 and 10 give the corresponding graphs for the soil and fluid loading terms in sandy and clay soils respectively. For the PVC water pipe, the fluid loading is heavy, Re(β) = 6, i.e. the fluid loading term in Eq. (31), Re($\beta/1-\nu_p^2$) $\gg 1$. Thus without the surrounding soil, the calculated propagation wavespeed is much less than the free-field fluid wavespeed c_f. The

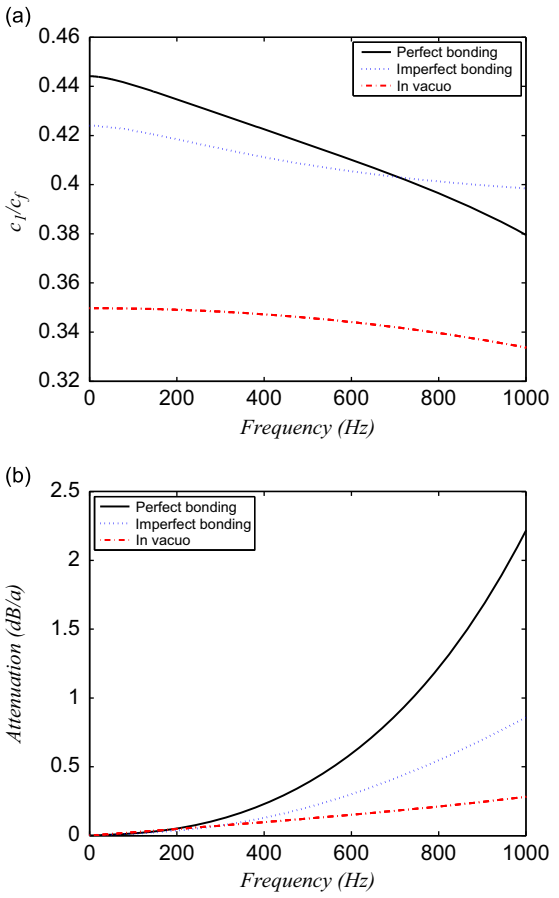

Fig. 9. Dispersion curves for the $s=1$ wave in a PVC water pipe buried in clay soil (B): (a) normalised wavespeed; (b) attenuation (dB/a).

real part of the soil loading term, Re(α), are found, in Figs. 8(a) and 10(a), to be similar to those observed with the cast iron pipe. The effects of the soil loading on the wavespeed are therefore similar (although slightly greater) than those observed with the cast iron pipe – a small increase compared with the corresponding *in vacuo* cases occurs, as shown in Figs. 7(a) and 9(a). As for the cast iron pipe, the wavespeed for "perfect bonding" is greater than that for "imperfect bonding" in particular at lower frequencies, as a result of the presence of the frictional stress at the interface. It should be noted that for heavy fluid loading, a slight underestimation may occur in the calculations of the $s=1$ wavespeed using Eq. (31).

Again, it is observed that the attenuation increases with frequency, but with significantly higher levels than for the cast iron pipe. This accords with what is found in practice: leak noise signals in plastic pipes are more heavily attenuated than those in metal pipes and, in consequence, of narrower bandwidth; this, in turn, dramatically limits the water leakage detection ranges for plastic pipes. Soil loading is found to have a considerable effect on the attenuation, particularly at higher frequencies, as shown in Figs. 8(b) and 10(b). At very low frequencies this effect, controlled by Im(α), is relatively small and losses within the pipe wall dominate; at higher frequencies Im(α) increases to a similar magnitude to Im(β). Similar to the cast iron pipe, for both bonding conditions, there is a greater increase of the attenuation for "perfect bonding" than for "imperfect bonding", in particular at higher frequencies.

In summary, for PVC pipes, the effect of soil loading needs be accounted for in the analysis of both the propagation wavespeed and wave attenuation.

5. Experimental work

Wavenumber measurements of the axisymmetric, fluid-dominated ($n=0$, $s=1$) wave in both in-air (to represent the *in vacuo* case) and buried fluid-filled plastic pipes have been made and reported previously [20,27]. For the *in vacuo* pipe, the measurements were found to agree well with the theory presented in [27]. For the buried pipe, the model of the wavenumber under lubricated contact (termed "imperfect bonding" in the present paper) was adopted to predict the real part of the wavenumber and the attenuation [20]. It was found that the real part of the wavenumber decreases relative to the in air case and good agreement was shown between the measurements and the predictions; however, the attenuation prediction

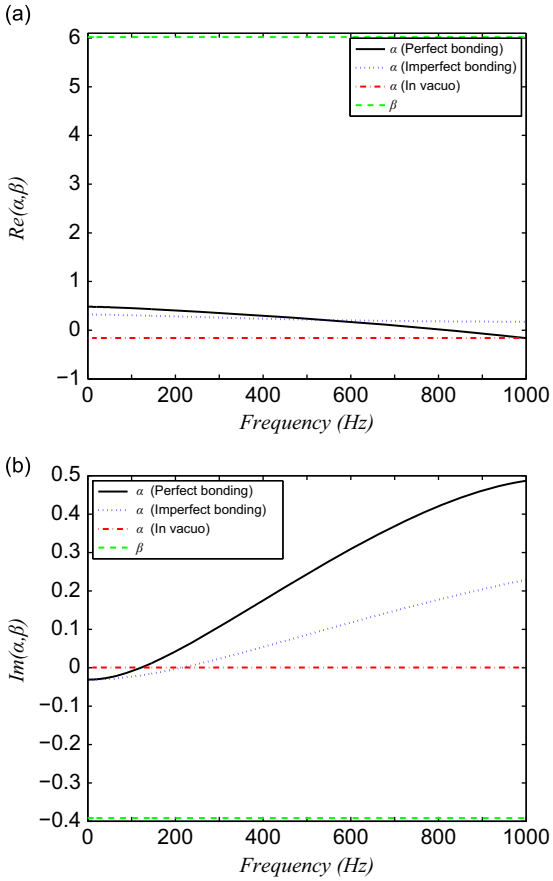

Fig. 10. Measures of the effects of soil and fluid loading, α and β, for a PVC water pipe buried in clay soil (B): (a) real part; (b) imaginary part.

gave a slight underestimate when compared with the measurements. This could be rectified by slightly altering the elastic modulus used in the predictions, but not without compromising the degree of agreement in the real part of the wavenumber. Here, the experimental results are again presented, in the light of the theory described in the current paper. The details of the experimental setup and analysis can be found in [27] and are not reproduced in detail here. However, the key features are highlighted. The test rig comprised a 34 m length, 180 mm diameter, MDPE pipe buried at a depth of approximately 1 m in loose, sandy soil, as shown in Fig. 11. The material properties assumed are given in Table 2. Measurements were made outside when the ground temperature was only a few °C, so the wavenumber predictions presented here are obtained by adopting the elastic modulus of MDPE at low-temperature as given in the table. The pipe was instrumented with a number of hydrophones along its length. It was excited with a modified moving-coil underwater loudspeaker mounted in a flange at one end of the pipe. The loudspeaker was excited with a stepped sine input from 30 Hz to 1 kHz at 1 Hz intervals. Signals from a pair of hydrophones spaced approximately 2 m apart were analysed in order to calculate the $s=1$ wavenumber in the buried pipe.

The real parts of the measured and predicted $s=1$ wavenumber and the corresponding attenuation are plotted in Fig. 12 (a) and (b) respectively. As can be seen from the figures, some fluctuations in both the real and imaginary parts of the measured results occur below 160 Hz; these are likely to be the result of reflections at the pipe ends and the various connections. Above 550 Hz the measured data becomes increasingly erratic and unreliable; this is probably associated with the "noise floor" being reached for the hydrophone pairs.

To evaluate the effect of frictional stress at the pipe–soil interface, wavenumber predictions are presented under both the "perfect bonding and "imperfect bonding" conditions. For the real part of the wavenumber, Fig. 12(a) shows that, the discrepancy in the predictions induced by the frictional stress is insignificant. There is a slight decrease (hence an increase of the wavespeed) under "perfect bonding" compared to "imperfect bonding", as expected in Section 4. The predictions are in good agreement with the experimentally measured results within the frequency range between 160 Hz and 550 Hz. A further check on the corresponding soil and fluid loading terms, as plotted in Fig. 13(a), reveals that for the test MDPE pipe, the fluid loading is very heavy, $\mathrm{Re}(\beta)=14.5$ compared to the real part of the soil loading term, $\mathrm{Re}(\alpha)$, as expected. Thus the effect of frictional stress is negligible in the calculation of the wavespeed.

For the wave attenuation, Fig. 12(b) shows that it increases under "perfect bonding" relative to "imperfect bonding" due to the effect of the frictional stress at the pipe–soil interface, as discussed in Section 4. Fig. 13(b) shows that the imaginary

Fig. 11. The test rig under construction [27].

part of the soil loading Im(α) increases with frequency, being greater for "perfect bonding". For heavy fluid loading, Im(β) is large compared with Im(α) at very low frequencies and thus losses within the pipe wall dominate; at higher frequencies both losses within the pipe and losses due to radiation contribute. It can be seen from Fig. 12(b) that good agreement is now achieved between the measurements and the predicted attenuation under "perfect bonding". This suggests that the fluid-filled pipe can be appropriately considered to be in perfect bond with the surrounding soil and, in order to be able to accurately predict the wave attenuation, the frictional stress at the pipe–soil interface must be properly taken into account.

Table 2
Properties of the MDPE pipe, soil and water.

Properties	MDPE	Soil	Water
a (m)	0.0845	–	–
h (m)	1.1e−2	–	–
Density (kg/m^3)	900	1500	1000
Young's modulus (N/m^2)	2.0e9	–	–
Bulk's modulus (N/m^2)	–	4e7	2.25e9
Shear modulus (N/m^2)	–	1.5e7	–
Poisson's ratio	0.4	–	–
Material loss factor	0.06	–	–

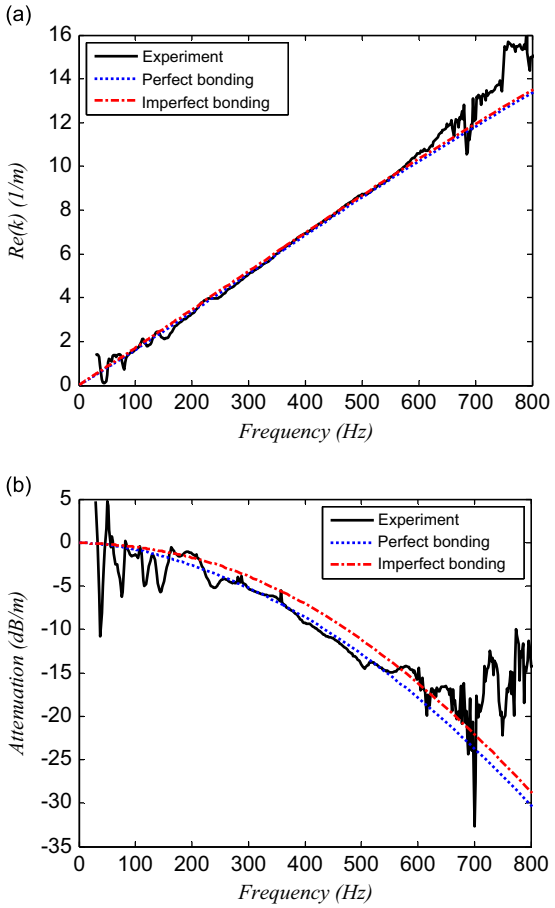

Fig. 12. Comparison of measured and predicted wavenumbers: (a) real part; (b) attenuation (dB/m).

6. Conclusions

The dispersion characteristics of the $n=0$, $s=1$ wave have been investigated in this paper. A simplified characteristic equation of a buried fluid-filled pipe has been established based on Donnell-Mushtari theory together with some simplifying assumptions confined to low frequencies. The effect of soil loading on the pipe response is characterised by introducing a soil loading matrix and the $s=1$ wavenumber has been derived with the frictional stress at the pipe–soil interface included.

Numerical results have shown that the fluid loading is the dominant factor in the prediction of the wavespeed. In particular, for light fluid loading, as is the case for metal pipes, the effect of soil loading can be neglected and the wave can be considered to be non-dispersive at low frequencies; for plastic pipes, the fluid loading is heavy and simply neglecting the effect of soil loading can lead to a slight underestimation in the calculation of the wavespeed. For both metal and plastic pipes, the soil loading adds damping to the coupled system, with the increase being more significant for the coupling case considered here, compared with the lubricated contact case studied previously. This effect increases with frequency and hence increases the wave attenuation more significantly at higher frequencies. The theory presented in this paper has been applied to wavenumber measurements

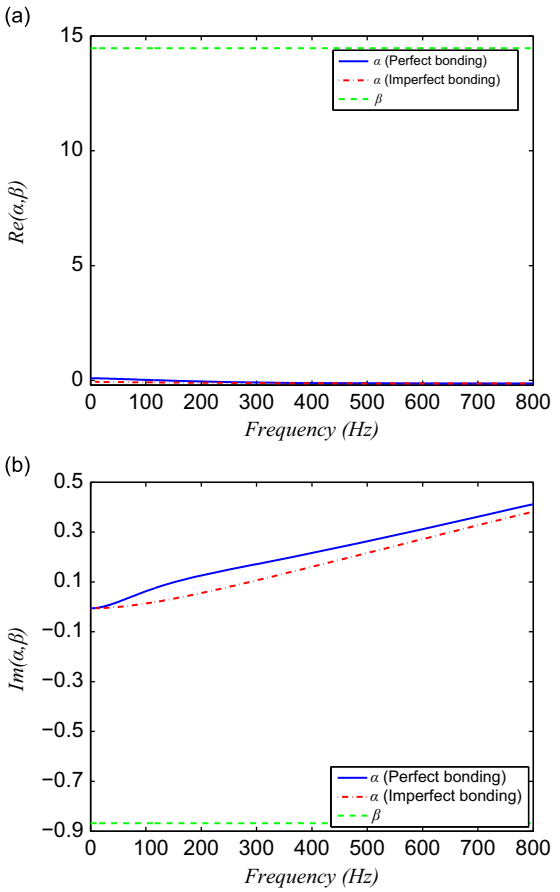

Fig. 13. Measures of the effects of soil and fluid loading, α and β, for the test MPDE water pipe: (a) real part; (b) imaginary part.

made on a buried MDPE water pipe. It has been found that although the wavespeed is not significantly affected by the inclusion of the frictional stress in the modelling, the wave attenuation increases markedly when the frictional stress is taken into account at the pipe–soil interface. The degree of agreement between prediction and experiment makes clear that the frictional stress need be properly accounted for in the attenuation predictions.

Acknowledgements

The authors acknowledge the support provided by the CAS Hundred Talents Programme and the EPSRC under EP/K021699/1. Many thanks are also due to Professor Mike Brennan and Dr. Paul Linford for allowing the experimental data acquired previously to be incorporated here. Data supporting this study are openly available from the University of Southampton repository at, read http://dx.doi.org/10.5258/SOTON/393627.

Appendix A. Properties of Bessel and Hankel functions

In this appendix, the properties of Bessel and Hankel functions used in the paper are given as follows [28]:

- For small argument $x \to 0$, $J_0(x)/J_0'(x) \approx -2/x$;
- For argument x, $H_1'(x) = H_0(x) - H_1(x)/x$ and $H_0'(x) = -H_1(x)$.

References

[1] H.V. Fuchs, R. Riehle, 10 years of experience with leak detection by acoustic-signal analysis, *Applied Acoustics* 33 (1991) 1–19.
[2] O. Hunaidi, W.T. Chu, Acoustical characteristics of leak signals in plastic water distribution pipes, *Applied Acoustics* 58 (1999) 235–254.
[3] J.M. Muggleton, M.J. Brennan, Y. Gao, Determining the location of buried plastic water pipes from measurements of ground surface vibration, *Journal of Applied Geophysics* 75 (2011) 54–61.

[4] B. Papandreou, M.J. Brennan, E. Rustighi, On the detection of objects buried at a shallow depth using seismic wave reflections, *Journal of the Acoustical Society of America* 129 (2011) 1366–1374.
[5] A. Demma, P. Cawley, M. Lowe, A.G. Roosenbrand, The reflection of the fundamental torsional mode from cracks and notches in pipes, *Journal of the Acoustical Society of America* 114 (2003) 611–625.
[6] R. Carandente, J. Ma, P. Cawley, The scattering of the fundamental torsional mode from axi-symmetric defects with varying depth profile in pipes, *Journal of the Acoustical Society of America* 127 (6) (2010) 3440–3448.
[7] M. Ratassepp, S. Fletcher, M.J.S. Lowe, Scattering of the fundamental torsional mode at an axial crack in a pipe, *Journal of the Acoustical Society of America* 127 (2010) 730–740.
[8] R. Kirby, Z. Zlatev, P. Mudge, On the scattering of longitudinal elastic waves from axisymmetric defects in coated pipes, *Journal of Sound and Vibration* 332 (2013) 5040–5058.
[9] R.J. Pinnington, A.R. Briscoe, Externally applied sensor for axisymmetrical waves in a fluid-filled pipe, *Journal of Sound and Vibration* 173 (1994) 503–516.
[10] Y. Gao, M.J. Brennan, P.F. Joseph, J.M. Muggleton, O. Hunaidi, A model of the correlation function of leak noise in buried plastic pipes, *Journal of Sound and Vibration* 277 (2004) 133–148.
[11] Y. Gao, M.J. Brennan, P.F. Joseph, A comparison of time delay estimators for the detection of leak noise signals in plastic water distribution pipes, *Journal of Sound and Vibration* 292 (2006) 552–570.
[12] M.J. Brennan, Y. Gao, P.F. Joseph, On the relationship between time and frequency domain methods in time delay estimation for leak detection in water distribution pipes, *Journal of Sound and Vibration* 304 (2007) 213–223.
[13] T.C. Lin, G.W. Morgan, Wave propagation through fluid contained in a cylindrical, elastic shell, *Journal of the Acoustical Society of America* 28 (1956) 1165–1176.
[14] J. Greenspon, Vibrations of thick and thin cylindrical shells surrounded by water, *Journal of the Acoustical Society of America* 33 (1961) 1321–1328.
[15] C.R. Fuller, F.J. Fahy, Characteristics of wave-propagation and energy-distributions in cylindrical elastic shells filled with fluid, *Journal of Sound and Vibration* 81 (1982) 501–518.
[16] B.K. Sinha, T.J. Plona, S. Kostek, S.K. Chang, Axisymmetrical wave-propagation in fluid-loaded cylindrical-shells. I. theory, *Journal of the Acoustical Society of America* 92 (1992) 1132–1143.
[17] A.W. Leissa, *Vibration of Shells, NASA SSP-288*, US Government Printing Office, Washington, DC, 1973.
[18] R. Long, P. Cawley, M. Lowe, Acoustic wave propagation in buried iron water pipes, *Proceedings of the Royal Society A* 459 (2003) 2749–2770.
[19] J.M. Muggleton, M.J. Brennan, R.J. Pinnington, Wavenumber prediction of waves in buried pipes for water leak detection, *Journal of Sound and Vibration* 249 (2002) 939–954.
[20] J.M. Muggleton, J. Yan, Wavenumber prediction and measurement of axisymmetric waves in buried fluid-filled pipes: Inclusion of shear coupling at a lubricated pipe/soil interface, *Journal of Sound and Vibration* 332 (2013) 1216–1230.
[21] J.M. Muggleton, M. Kalkowski, Y. Gao, E. Rustighi, A theoretical study of torsional waves in buried pipes for pipeline condition assessment and monitoring, *Journal of Sound and Vibration* (2016) (in press).
[22] H. Jia, M. Jing, L.R. Joseph, Guided wave propagation in single and double layer hollow cylinders embedded in infinite media, *Journal of the Acoustical Society of America* 129 (2) (2011) 691–700.
[23] T. Akiyoshi, K. Fuchida, Soil–pipeline interaction through a frictional interface during earthquakes, *Soil Dynamics and Earthquake Engineering* 3 (1) (1984) 27–34.
[24] Y. Nassira, H. Rajaie, R.T. Faal, Three dimensional vibration analysis of a buried pipeline with slip conditions, *Soil Dynamics and Earthquake Engineering* 31 (2011) 1629–1639.
[25] W.M. Ewing, W.S. Jardetzky, F. Press, *Elastic Waves in Layered Media*, McGraw-Hill, New York, 1957.
[26] D.I. Korteweg, Über die Fortpflanzungsgeschwindigkeit des Schalles in elastischen Röhren (On the speed of sound in water in flexible pipes), *Annalen der Physik* 5 (1878) 525–542.
[27] J.M. Muggleton, M.J. Brennan, P.W. Linford, Axisymmetric wave propagation in fluid-filled pipes: wavenumber measurements in in vacuo and buried pipes, *Journal of Sound and Vibration* 270 (2004) 171–190.
[28] M. Abramowitz, I.A. Stegun, *Handbook of Mathematical Functions*, Dover publications, New York, 1970.